Journal of Science and Transport Technology
Journal homepage: https://jstt.vn/index.php/en

Durability of reinforced geopolymer concrete using coral aggregates and seawater under accelerated corrosion

Le Hong Quan*, Tran Van Tuan, Dong Van Kien, Nguyen Van Chi, Cao Nhat Linh, Nguyen Van Trieu, Nguyen Duc Anh
Coastal Branch of the Joint Vietnam - Russia Tropical Science and Technology Research Center, Nha Trang, Vietnam

Article info
Type of article:
Original research paper

DOI:
https://doi.org/10.58845/jstt.utt.2026.en.6.1.1-14

***Corresponding author:**
Email address:
quanttndvn@gmail.com

Received: 09/05/2025
Received in Revised Form: 25/09/2025
Accepted: 27/01/2026

Abstract: This study evaluates the corrosion resistance of geopolymer concrete made with coral sand, coral rock, and seawater, materials abundant on offshore islands. Three mixtures were designed using varying proportions of fly ash and blast furnace slag as binders. Compressive strengths after 28 days were 20.11 MPa, 25.32 MPa, and 30.15 MPa for GPS-1, GPS-2, and GPS-3, respectively. Accelerated corrosion tests (NT Build 356) revealed that higher strength samples exhibited lower average current intensity before cracking (5.49 mA for GPS-1 vs. 4.68 mA for GPS-3) and longer times to cracking (204 h vs. 324 h). Chloride ion concentrations near the steel at the onset of cracking were similar across mixtures (0.53 % – 0.58 % by dry concrete weight), but initial chloride contents were lower in high-strength samples (0.08 % in GPS-3 vs. 0.22 % in GPS-1), indicating better resistance to ion penetration. Microstructural analyses (SEM, FTIR, XRD) confirmed that GPS-3 had a denser matrix, more developed geopolymer gel, and reduced presence of unreacted crystalline phases. These results demonstrate that optimizing binder content and microstructure enhances both mechanical performance and corrosion resistance, making geopolymer concrete with marine-derived materials a viable solution for durable coastal infrastructure.

Keywords: Geopolymer concrete, coral sand, seawater, chloride penetration, steel corrosion, NT Build 356.

1. Introduction

Infrastructure development on offshore islands in Vietnam has garnered noteworthy attention and substantial progress over the recent years. One of the primary challenges associated with large-scale construction projects on the islands pertains to transporting materials from the mainland. This process not only escalates construction costs but also prolongs the construction duration while concurrently contributing to heightened energy consumption. In the offshore islands, coral sand is the predominant variety [1-3]. Therefore, leveraging this particular sand type to replace river sand in concrete production could offer numerous benefits.

Sea sand and seawater have been previously studied for use in cement concrete [4-7]. Both sea sand and seawater contain high levels of sulfate and chloride, the two main factors responsible for damaging concrete structures and corroding steel reinforcement. Studies indicate that the presence of carbonate ions in Poclang cement concrete can lead to the formation of Thaumasite ($CaSiO_3.CaCO_3.CaSO_4.15H_2O$) due to the reaction

of calcium silicate hydrate (C–S–H) and sulfate, resulting in cracking, softening, and reduced durability [8-10]. Several studies have demonstrated that using sulfate-resistant cement can help mitigate the drawbacks. However, in concrete that utilizes sulfate-resistant cement, chloride ions bind to sulfate and tricalcium aluminate, forming calcium chloroaluminate ($3CaO.Al_2O_3.CaCl_2.10H_2O$) [11-13]. This compound can release chloride ions, which may migrate through the pores and reach the steel surface. To prevent potential issues, washing sea sand to remove chloride and salt content is recommended, which may increase construction costs.

Recently, geopolymer concrete has been gaining interest because it aims to create an eco-friendly production process by reducing CO_2 emissions and utilizing industrial waste such as ash, slag, and red mud [14-16]. Geopolymer is characterized by its dual nature, combining the characteristics of a polymer (such as allotropy transformation, polymerization, and low-temperature curing) with those of an inorganic compound (being durable and stable at high temperatures, and resistant to combustion) [17-19]. There are nine types of geopolymers, but the ones most commonly used in construction are derived from silicon and aluminum (aluminosilicate) [15,20,21]. Their main polymerization products generally do not include portlandite or C–S–H formation, significantly reducing the risks associated with sulfate attack [22-26]. Therefore, using coral sand and seawater as replacements for river sand and fresh water in geopolymer concrete is an option worth exploring [10,27-33].

Previous studies have primarily focused on the mechanical properties of geopolymer concrete containing partial coral aggregates. However, research on the corrosion of reinforcement in geopolymer concrete made with entirely coral aggregates and seawater is quite limited. Therefore, this study aims to develop and evaluate geopolymer concrete that uses entirely coral aggregates and seawater, specifically examining its mechanical performance, microstructure, and corrosion resistance. The presence of inherent chloride ions in the raw materials poses a unique challenge for evaluating durability. In this context, conventional assessment methods such as half-cell potential (ASTM C876) and surface resistivity (AASHTO TP 95) may yield ambiguous results. This technique is based on the measurement of corrosion potential, which can be significantly influenced by the ionic conductivity of the pore solution and the presence of chlorides. In saline systems, the measured potential may appear more negative not necessarily due to active corrosion, but rather due to enhanced electrolyte conductivity, leading to potential misinterpretation. Instead, accelerated corrosion testing using impressed voltage (NT Build 356) offers a more appropriate means of evaluating corrosion progression [34]. This technique enables the quantification of time to cracking and corrosion rate under controlled chloride exposure. Moreover, by measuring total chloride content in the vicinity of the steel reinforcement at the time of cracking, it becomes possible to estimate the critical chloride threshold for passivity breakdown, an essential parameter in geopolymer systems where chloride is already present in the mix. When combined with phase and microstructural analysis tools such as X-ray diffraction (XRD), Fourier-transform infrared spectroscopy (FTIR), and SEM, this method provides a comprehensive understanding of corrosion mechanisms in geopolymer concretes formulated with coral sand and seawater.

The uniqueness of this research lies in the use of local materials in the Truong Sa Islands to create cement-free concrete, aiming to provide sustainable infrastructure solutions for remote island applications.

2. Experimental

2.1. Material

Fly ash (FA) and blast furnace slag (BFS) are binding agents, with their chemical compositions

detailed in Table 1. Sodium hydroxide (NaOH, 99 %) and liquid glass ($Na_2SiO_3.5H_2O$, Modulus Ms: 2.3 ÷ 2.8) were combined to create an alkaline activation solution, all purchased from Vietnam.

Table 1. Chemical composition of FA and BFS

Material	Chemical composition (wt.%)											
	SiO_2	Al_2O_3	Fe_2O_3	CaO	MgO	Na_2O	SO_3	TiO_2	K_2O	MnO	P_2O_5	LOI
FA	65.34	25.49	3.67	1.61	0.6	0.48	0.21	0.34	0.39	0.03	0.073	0.94
BFS	33.92	10.45	0.39	40.6	6.55	0.4	0.04	0.43	0.71	-	-	0.12

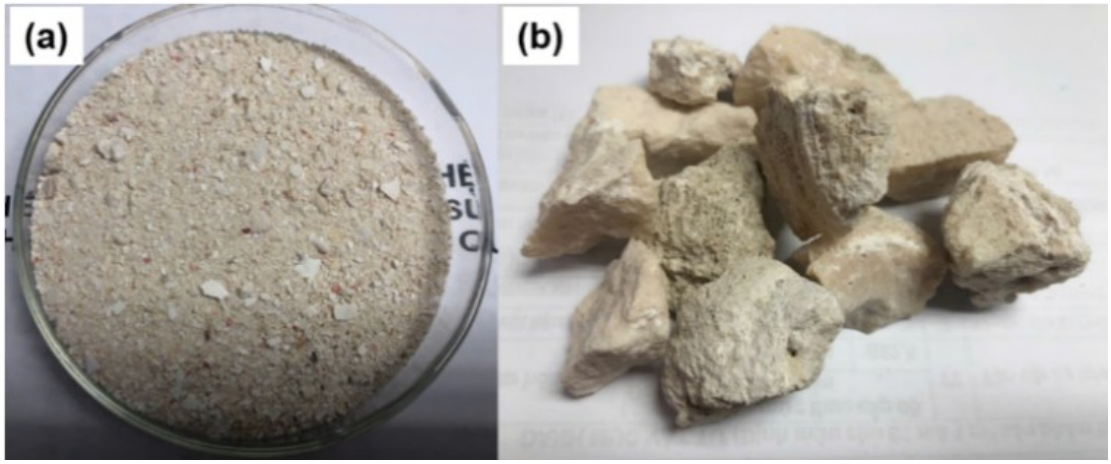

Fig. 1. (a) coral sand, (b) coral rock

Table 2. Properties of aggregate

Properties	Coral rock	Coral sand
Apparent density, kg m^{-3}	2113	2343
Bulk density, kg m^{-3}	976	1285
Cl- content, %	0.013	0.011

Table 3. Parameters of seawater

Salinity, ‰	pH	Mg^{2+}, ppm	Ca^{2+}, ppm	Na^{2+}, ppm	Cl^-, ppm
33,1	8,3	1210	389	11036	18512

The aggregate consists of (10 x 20) mm coarse aggregate made from crushed coral rock and fine aggregate made from coral sand (Fig. 1). The physical and chemical properties of the aggregates are detailed in Table 2. The parameters of seawater are shown in Table 3. The materials were gathered from the Truong Sa Islands in Vietnam.

Steel reinforcements with a diameter of 12 mm are utilized and cleaned with acetone before embedding in concrete. These steel reinforcements are produced by the Hoa Phat Steel factory in Vietnam.

2.2. Mix design and mixing

Before proceeding, it is essential to prepare the alkaline activator solution. First, mix sodium hydroxide powder with tap water to create a 12M NaOH solution. Next, add liquid glass to the 12M NaOH solution in a mass ratio of 1.5:1 and stir thoroughly. Prepare this solution 24 hours before application to ensure it cools to room temperature.

The three concrete mixtures created for the research are outlined in Table 4. Mix the aggregate with water and a water-reducing admixture for three minutes. Then, add the FA and BFS binder, mixing for an additional two minutes. Finally, incorporate the active alkali solution and mix thoroughly for two minutes.

The three concrete mixtures created for the research are outlined in Table 4. Mix the aggregate with water and a water-reducing admixture for three minutes. Then, add the FA and BFS binder,

mixing for an additional two minutes. Finally, incorporate the active alkali solution and mix thoroughly for two minutes.

For each test, three replicate specimens were prepared for every mix. The corrosion tests used cylindrical samples of size Ø100 x 300 mm, which included Ø12 x 200 mm reinforcement embedded in the concrete. The compression tests utilized samples of size 15 x 15 x 15 cm.

The mixed mortar is poured into molds and then compressed using a vibrator for about 1 minute until it reaches a visually uniform state within the mold. The samples were kept at 23 °C with 95 % humidity and were removed from the mold after 48 hours.

2.3. Test methods and characterization

The concrete compressive strength test was conducted using a TYA-2000 compression apparatus.

The accelerated corrosion test method for steel reinforcement follows the NT Build 356 standards. The experimental diagram is illustrated in Fig. 2. The samples were submerged in seawater, with the sample surface positioned 30 mm above the solution's top level. A constant potential of 5V was applied across the samples, with the steel reinforcement serving as the anode and the stainless steel plate as the cathode.

Table 4. Concrete mixtures

Mix type	Binding agents			Alkaline activation solution, kg	Aggregate			Seawater, kg	Superplasticizer, kg
	Total weight, kg	FA, kg	BFS, kg		Total weight, kg	fine aggregate, kg	coarse aggregate, kg		
GPS-1	400	280	120	160	1840	662	1204	80	4
GPS-2	440	308	132	176	1784	643	1170	80	4.4
GPS-3	480	336	144	192	1728	625	1135	80	4.8

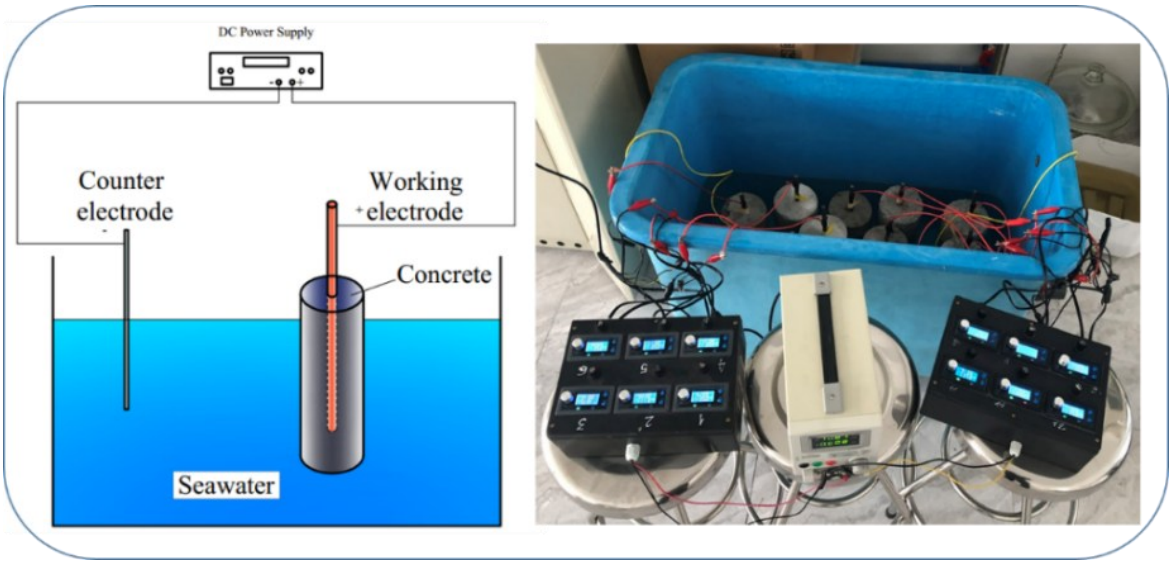

Fig. 2. Schematic diagram of an accelerated corrosion experiment

This study proposes an accelerated electrochemical corrosion testing procedure for reinforced concrete structures, consisting of five basic steps:

Step 1: At 28 days old, the concrete test samples are submerged in a seawater tank for at least 48 hours. This ensures that all samples are thoroughly saturated with seawater and allows chloride ions to diffuse into the concrete.

Step 2: Connect the steel reinforcement of

the test samples to a transformer following the parallel circuit diagram.

Step 3: Experiment to accelerate the corrosion of steel reinforcement using electrochemical methods. Record the current displayed on the transformer every 6 hours for the first 2 days and every 12 hours for the following days during the experiment.

Step 4: Complete the test to accelerate steel reinforcement corrosion using the electrochemical method until the concrete cracks.

At the time of concrete cracks, determine the total Cl^- content near the steel reinforcement following the ASTM C1152. Approximately 1 g of finely ground sample was dissolved in 50 mL of 1M nitric acid (HNO_3) under gentle heating and continuous stirring. The resulting solution was filtered and titrated with a standardized silver nitrate ($AgNO_3$) solution using potassium chromate (K_2CrO_4) as an indicator.

The morphologies of samples were characterized using an SEM (S-4800, Hitachi). The phase composition was examined using XRD under Cu Kα radiation (X'Pert-PRO MPD, PANalytical). Determine the chemical structure by FTIR from 600 to 4000 cm^{-1} at a resolution of 16 cm^{-1} for 32 scans (NicoletiS10, Thermo Scientific).

3. Results and discussion

3.1. Compressive strength

After 28 days of sample curing, the compressive strength of each geopolymer concrete using coral sand and seawater mixture was tested. The compressive strength values of GPS-1, GPS-2, and GPS-3 were 20.11, 25.32, and 30.15 MPa, respectively (Fig. 3a). The increase in compressive strength is attributed to the improved geopolymerization process and the more refined microstructure resulting from higher proportions of FA and BFS. These results suggest that adjusting the binder composition significantly influences the development of a denser matrix and a stronger internal bond. Fig. 3b illustrates the internal structure of the concrete sample and shows strong bonding between the binder and coral aggregate. Most large aggregates were broken rather than separated from the binder after damage.

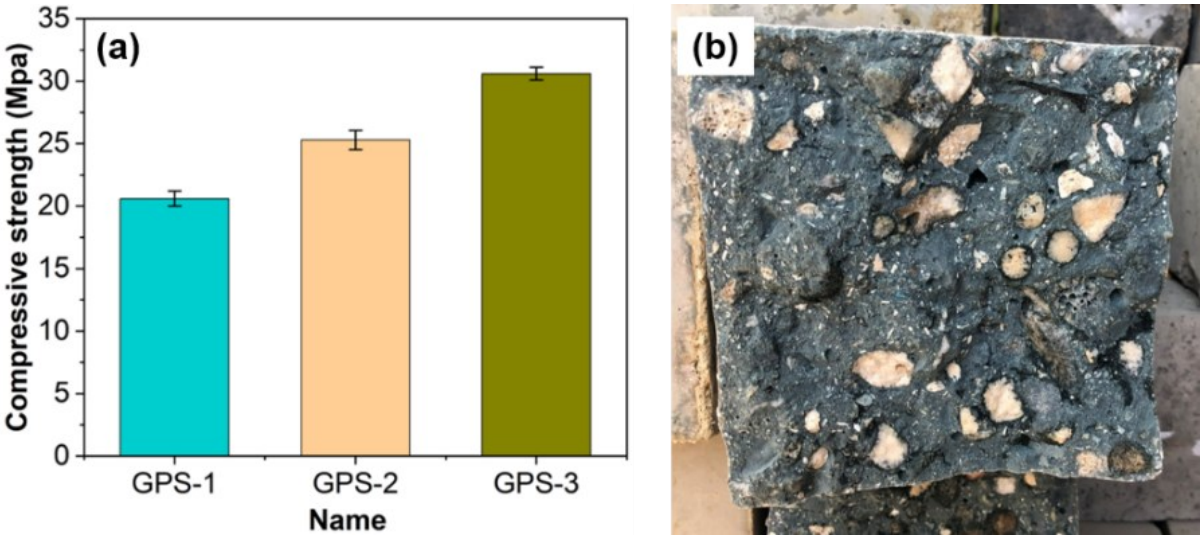

Fig. 3. (a) Compressive strength of the samples, (b) The internal structure of concrete

3.2. Accelerated corrosion tests

Fig. 4 presents the variation in current intensity over time for each GPS sample under accelerated corrosion testing. From the early stages of measurement, samples with higher compressive strength, particularly GPS-3 exhibited consistently lower current intensity values. Specifically, on the first day, the current intensities recorded were 5 mA for GPS-1, 4 mA for GPS-2, and 3 mA for GPS-3. The average current intensities prior to cracking were 5.49, 4.76, and 4.68 mA, respectively. These values suggest that concrete specimens with higher compressive strength provide more effective resistance against

ionic conductivity and electrochemical corrosion processes.

The observed trend, where current intensity decreased as compressive strength increased is closely associated with the material's ability to limit chloride ion ingress. This correlation is supported by chloride content measurements (Table 5), which show that at the initial stage of exposure, the total Cl^- content around the steel in GPS-1, GPS-2, and GPS-3 was 0.22 %, 0.12 %, and 0.08 % by dry concrete weight, respectively. The lower initial chloride content in higher-strength samples indicates a denser geopolymer gel network with enhanced chloride-binding capacity and reduced pore connectivity, thus lowering ionic mobility and electrochemical activity.

As the test progressed, a sharp increase in current intensity was observed at the moment of cracking for each sample, with values of 19.33 mA (GPS-1), 17.67 mA (GPS-2), and 17.33 mA (GPS-3), occurring at 204, 264, and 324 hours, respectively. Since all specimens used the same type and size of reinforcement, a significant accumulation of Cl^- ion around the reinforcement is necessary for corrosion to occur, which can eventually lead to failure. At the time of cracking in the specimens, the total chloride ion content was similar across all samples (0.53 % ÷ 0.58 % Cl^-). However, specimen GPS-3 had the lowest initial total Cl^- ion content. Its high strength likely slowed the permeation of Cl^- ion, resulting in GPS-3 requiring more time to reach the failure point.

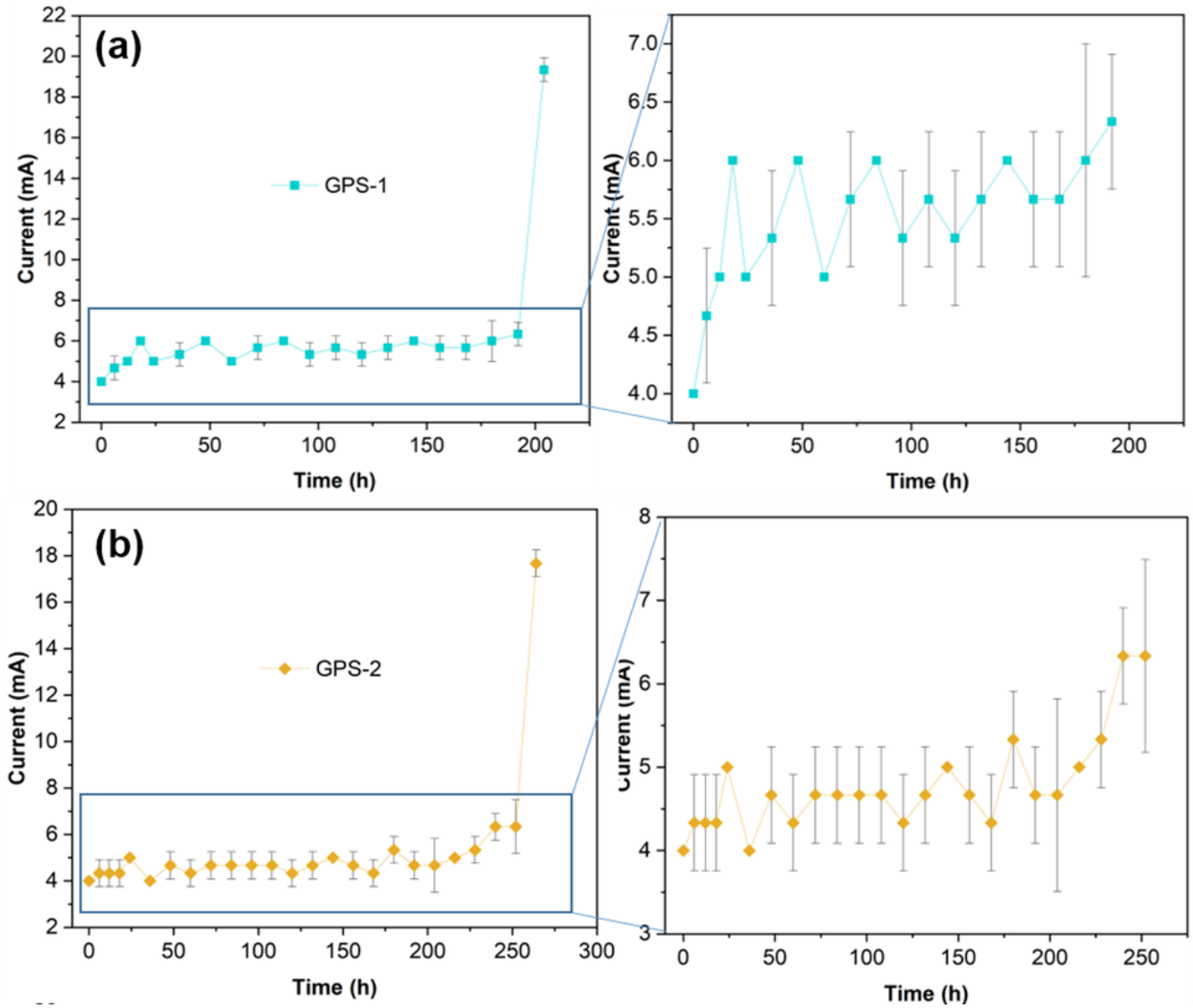

Fig. 4. Current at the time of the test

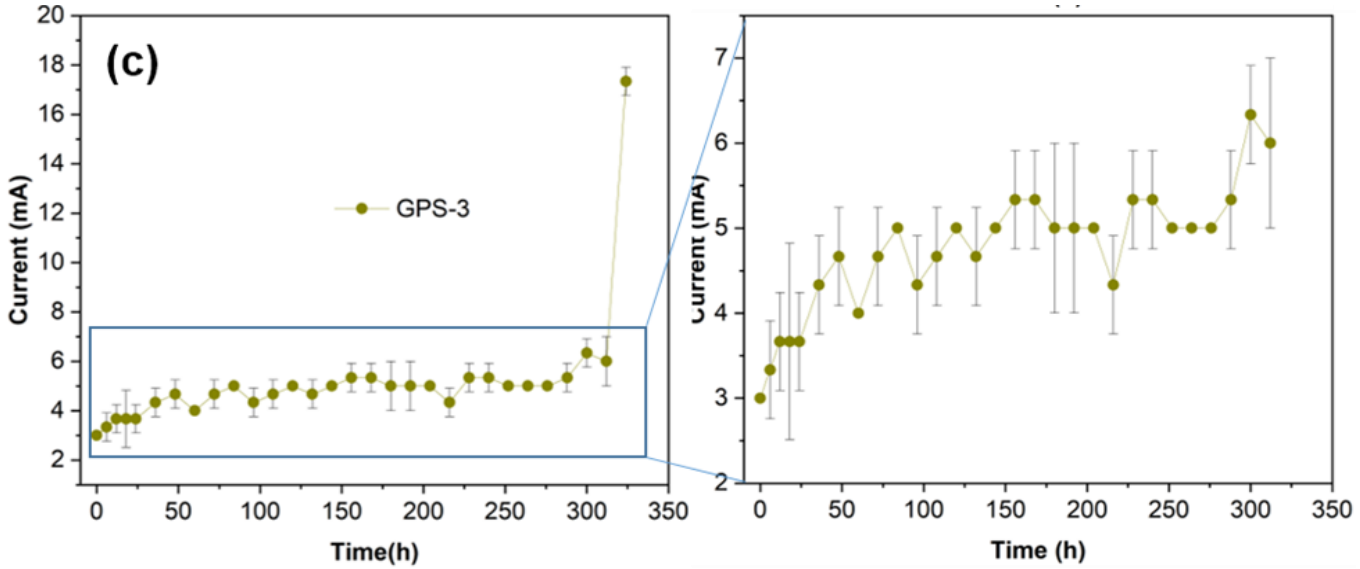

Fig. 4. (continued)

Table 5. The total ion Cl^- content in the reinforcement area and the time of crack appearance

Mix type	Initial Cl^-, (% by dry concrete weight)	Cl^- at the time of crack (% by dry concrete weight)	Time, Hour
GPS-1	0.22 ± 0.006	0.58 ± 0.015	204
GPS-2	0.12 ± 0.015	0.54 ± 0.015	264
GPS-3	0.08 ± 0.006	0.53 ± 0.006	324

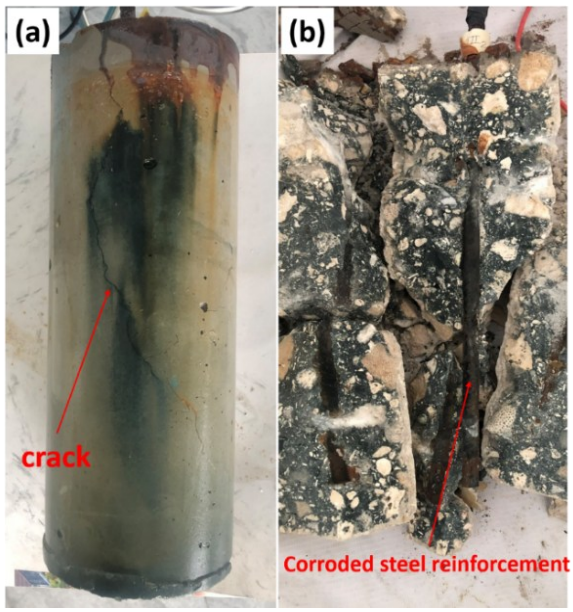

Fig. 5. (a) Image at the time of cracking; (b) Steel reinforcement at the time of cracking

At the time of sample cracking, the surface of the samples exhibited cracks in the protective concrete layer in the direction of the steel bars, accompanied by the presence of steel corrosion products (Fig. 5a). Chloride ions from seawater can penetrate concrete through its pores and cracks. This process can damage the passive film that protects the steel reinforcement, forming corrosion products such as $Fe(OH)_3$ or Fe_2O_3 (Fig. 5b).

Overall, these findings reveal a strong coupling between compressive strength, chloride ion distribution, and current intensity during corrosion. Improving the gel structure of geopolymer concrete not only reduces chloride accumulation near embedded steel but also suppresses current flow, delaying reinforcement

corrosion and improving long-term durability in marine environments. To further elucidate these correlations, advanced characterization techniques such as SEM, FTIR, and XRD were employed in this study.

3.3. Microstructural and phase analysis

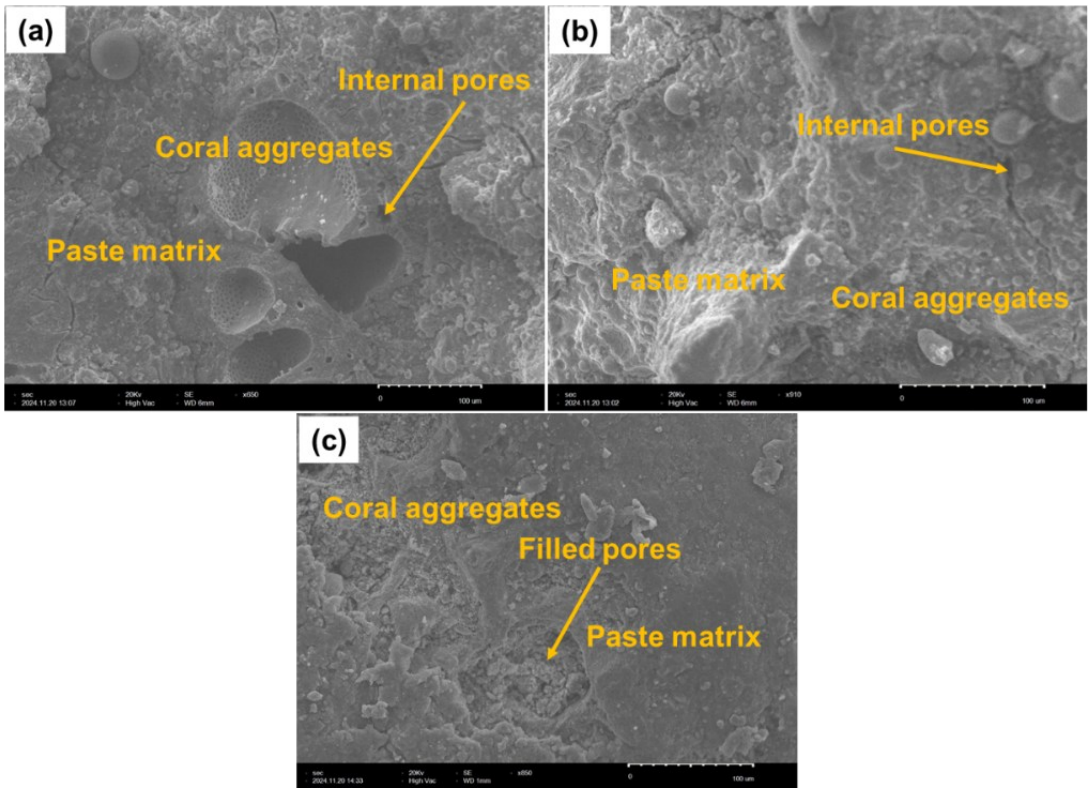

Fig. 6. SEM images of (a) GPS-1, (b) GPS-2, and (c) GPS-3

SEM analysis (Fig. 6) revealed that specimens with higher compressive strength (GPS-3) exhibited notably denser interfacial transition zones (ITZs) and a lower density of microcracks.

The geopolymer gels in these samples appeared well-compacted and strongly bonded to the porous coral aggregates, suggesting that the improved mechanical performance was closely associated with enhanced pore refinement and a more cohesive aggregate–matrix interface. Although Fig. 3b shows that coral aggregates fractured even in GPS-1, suggesting a relatively strong ITZ at the macroscale, this fracture mode is also heavily influenced by the inherently porous and brittle nature of the coral aggregates themselves. The SEM analysis (Fig. 6a) confirms that at the microscale, the ITZ of GPS-1 is indeed weaker and less continuous compared to GPS-2 (Fig. 6b) and GPS-3 (Fig. 6c). SEM images also revealed that GPS-1 exhibits more micro-cracks and less continuous gel around the aggregate surface. These microstructural features are consistent with the comparatively lower mechanical and durability performance of GPS-1. This microstructural vulnerability also likely contributed to the inferior chloride ion resistance observed in GPS-1, as compared to the superior performance of GPS-2 and GPS-3.

Fig. 7a presents the FTIR spectra of the same samples, highlighting notable differences in the position of the characteristic Si–O–T (T = Si or Al) asymmetric stretching vibration band within the 950 ÷ 1000 cm-1 region. Specifically, sample GPS-1 exhibited its absorption peak at 1006 cm-1, while GPS-2 and GPS-3 showed peaks at 998 cm-1 and 954 cm-1, respectively. A shift toward lower wavenumbers is typically associated with the progressive substitution of Al for Si within the silicate framework, leading to the formation of more Si–O–Al linkages characteristic of more extensively polymerized aluminosilicate gel

networks [15,35].

This observation suggests that the sample GPS-3 achieved higher geopolymerization, forming a more continuous and stable gel structure. In contrast, the relatively higher wavenumber of 1006 cm-1 in GPS-1 implies a predominance of Si–O–Si linkages, reflecting either incomplete geopolymerization or the presence of unreacted silicate species, which may contribute to a more heterogeneous and porous microstructure. These findings are consistent with previous studies that report that FTIR peak shifts toward lower wavenumbers are reliable indicators of more advanced geopolymer gel formation and improved performance in aggressive environments [36,37]. Absorptions peak at 3300 ÷ 3500 cm-1 and 1640 cm-1 correspond to the O–H stretching and H–O–H bending vibrations associated with physically adsorbed water or hydroxyl groups within the gel matrix. In addition to the leading bands related to geopolymer gel formation, the FTIR spectra of the samples also exhibit several characteristic absorption peaks (1420 cm-1) corresponding to carbonate groups (CO32-), which are clear indicators of the presence of calcium carbonate (CaCO3), the principal mineral component of coral sand. These bands are most intense in GPS-1, implying a higher moisture content and less condensed gel, which supports the observation of incomplete geopolymerization in this sample. Therefore, based on both chloride ion penetration measurements and FTIR spectral analysis, it can be concluded that sample GPS-3 possesses a more chemically stable structure and is likely to exhibit higher mechanical strength and improved durability against chloride-induced deterioration in marine environments.

Fig. 7b presents the XRD patterns of GPS-1, GPS-2, and GPS-3. All samples exhibit diffraction peaks at 2θ of 29, 36, 39, 43, 48, 50, and 54, which are primarily attributed to residual crystalline phases such as calcite ($CaCO_3$), quartz (SiO_2), and aluminosilicates. However, notable variations in peak intensity and sharpness are observed among the samples, suggesting differences in the extent of reaction and phase transformation.

To better assess the development of amorphous gel, Fig. 7c shows the XRD patterns in the range of 15° ÷ 35°, where a broad hump typically signifies the presence of geopolymeric gel (N-A-S-H or C-A-S-H). GPS-1 exhibits a relatively flat and low-intensity background within 15° ÷ 25°, alongside sharp and intense crystalline peaks at ~26.5°, 29.4°, and 31.5°. This indicates that most precursor minerals remain unreacted, reflecting a limited degree of geopolymerization. In contrast, GPS-3 shows a well-developed amorphous hump in the same region and noticeably reduced crystalline peak intensity. This pattern suggests significant dissolution of raw materials and the successful formation of an amorphous gel matrix, indicative of a more complete geopolymerization process. GPS-2 demonstrates intermediate characteristics, with a moderately developed amorphous background and less intense crystalline peaks than GPS-1. These findings clearly illustrate a progressive improvement in geopolymerization from GPS-1 to GPS-3. The degree of amorphous phase formation is positively correlated with the reduction of unreacted crystalline phases and is consistent with the observed trend in mechanical performance. The analytical results confirmed that the GPS-3 sample, which has a denser gel matrix and improved chloride ion binding capacity, slowed the corrosion initiation and extended the concrete's service life. Notably, the typical deleterious crystalline phases linked to sulfate and chloride attacks such as $Ca(OH)_2$, ettringite, and Friedel's salt were either completely absent or present only in trace amounts in the GPS samples. Instead, the presence of Chlorkyugenite ($Ca_{12}Al_{14}O_{32}Cl_2.4H_2O$, PDF 00-066-0640) phase indicates the chloride immobilization capability of geopolymer concrete made with a combination of fly ash and blast furnace slag. This suggests that the binding of chlorides in geopolymer concrete occurs through chemical interactions within the aluminosilicate

matrix, even in the absence of Friedel's salt. In addition, the compact pore structure of GPS effectively restricted the ingress of external ions, thereby limiting secondary reaction pathways and reducing the potential for internal microstructural damage.

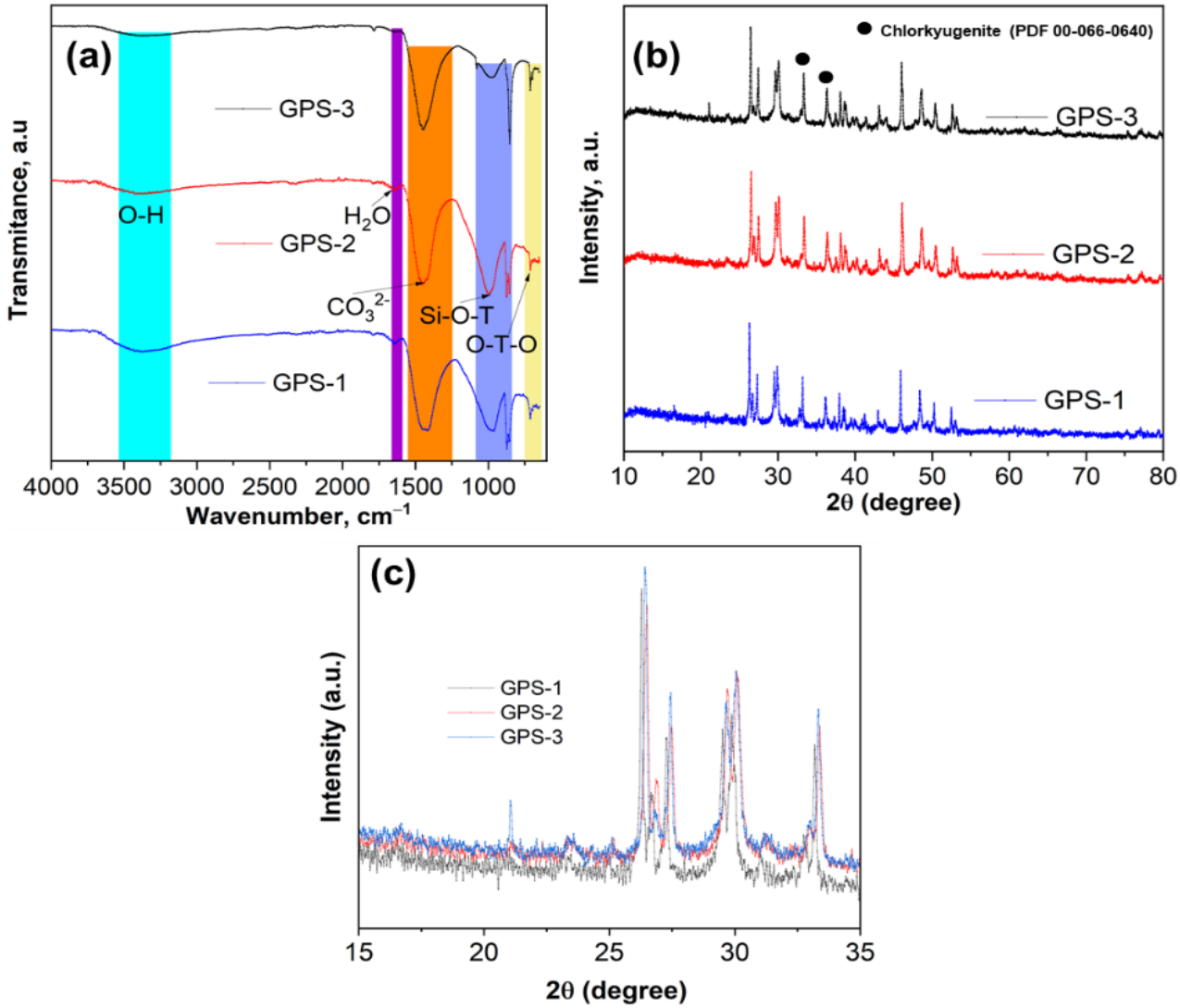

Fig. 7. (a) FTIR spectra of GPS; (b) XRD pattern of GPS samples, (c) XRD patterns in the range of 15° ÷ 35°

3.4. General discussion on mechanisms governing durability

The experimental results demonstrate a clear relationship between compressive strength, microstructural development, chloride resistance, and steel corrosion in the geopolymer concrete mixtures. The GPS-3 mixture, which exhibited the highest compressive strength at 30.15 MPa, also showed a denser gel network, lower total porosity, and decreased chloride ingress. These findings were confirmed by FTIR, XRD, SEM, and porosity analyses. The enhanced microstructural characteristics of the GPS-3 mixture contributed to a delayed onset of corrosion, reduced corrosion current intensities.

An important clarification lies in distinguishing between the chloride resistance of the concrete matrix and the critical chloride threshold at the steel–concrete interface. The results show that although the critical chloride threshold at the onset of cracking was essentially constant across all mixtures (0.53–0.58%), the time to cracking and the overall microstructural integrity were markedly superior in GPS-3. This apparent inconsistency is resolved when the two concepts are properly separated. Chloride

resistance is a kinetic property of the bulk material, governing the rate of ion transport through the pore network. The denser and more refined microstructure of GPS-3, as evidenced by SEM, FTIR, and XRD, provides a superior barrier against chloride ingress, thereby prolonging the time to cracking (324 h for GPS-3 compared with 204 h for GPS-1). In contrast, the critical chloride threshold is an electrochemical property at the steel–concrete interface, defined as the minimum chloride concentration required to depassivate the passive film on the reinforcement. Since all mixtures share the same geopolymer chemistry and establish a comparably high-pH environment around the steel, the passive film formed is chemically similar, resulting in a nearly identical chloride threshold across mixtures. In summary, while the condition for corrosion initiation remains constant, the optimized microstructure of GPS-3 significantly delays the attainment of this condition, thereby extending the initiation phase and providing the mechanistic basis for the enhanced durability and service life observed in this mixture.

The geopolymer matrix in this study immobilized chloride ions through a combination of physical entrapment, electrostatic interactions, and the formation of secondary calcium-aluminate-chloride phases, such as Chlorkyugenite (Ca-Al-O-Cl, PDF 00-066-0640). Overall, geopolymer concrete that incorporates marine-derived materials offers a promising solution for improving the durability of reinforced structures in coastal and island environments. This type of concrete may be well-suited for marine applications, such as protective structures, breakwaters, and secondary load-bearing components, where durability is more important than achieving high compressive strength. Future studies should investigate corrosion progression beyond initial cracking and evaluate the residual mechanical performance of steel reinforcement under long-term exposure.

4. Conclusions

This study demonstrates that geopolymer concrete made with coral sand, coral rock, and seawater can offer enhanced mechanical strength and corrosion resistance when properly optimized. Among the three mixtures, GPS-3 with the highest binder content achieved the greatest compressive strength (30.15 MPa) and exhibited superior durability under accelerated corrosion testing. This sample showed the lowest initial chloride content near the steel (0.08 % by binder mass), the lowest average current intensity before cracking (4.68 mA), and the longest time to crack formation (324 hours). Microstructural analyses confirmed that its improved performance was attributed to a denser matrix, more developed geopolymer gel, and reduced presence of reactive crystalline phases. The findings highlight that increasing binder content and promoting gel polymerization significantly improve chloride resistance and delay steel corrosion. Thus, geopolymer concrete incorporating marine-derived materials is a promising solution for enhancing the durability of reinforced structures in coastal and island environments.

Acknowledgments

This research is funded by the Joint Vietnam - Russia Tropical Science and Technology Research Center under grant number VB.Đ1.03/23.

References

[1] D.T. Pham, T.L. Nguyen, V.T. Vu, N.H. Tran. (2024). Research solutions for precast concrete revetments using alb-rebar to retain coral sand for offshore islands in Vietnam. *Journal of Science and Technique*, 7(1), 60-72. DOI: 10.56651/lqdtu.jst.v7.n01.830.sce

[2] N.X. Bang, N.T. Ta, T.V. Cuong, L.H. Duong, P.A. Vu. (2023). Determination of the mechanical properties of coral material used as concrete aggregates (in Vietnamese). *Journal of Construction*, 9, 78-81.

[3] W. Wang, B. Wang, L. Shen, C. Fan. (2024). Properties of Fly Ash Geopolymer Concrete as Marine Artificial Reef Building Materials. *Journal of Materials in Civil Engineering*, 36(2), 04023548.https://doi.org/10.1061/JMCEE7.MT

ENG-16541

[4] F. Yu, S. Dong, L. Li, A. Ashour, S. Ding, B. Han, J. Ou. (2023). Developing a Sustainable Ultrahigh-Performance Concrete Using Seawater and Sea Sand in Combination with Superfine Stainless Wires. *Journal of Materials in Civil Engineering*, 35(10), 04023368. https://doi.org/10.1061/JMCEE7.MTENG-16072

[5] T. Dhondy, A. Remennikov, M. Neaz Sheikh. (2020). Properties and Application of Sea Sand in Sea Sand–Seawater Concrete. *Journal of Materials in Civil Engineering*, 32(12), 04020392.https://doi.org/10.1061/(ASCE)MT.1943-5533.0003475

[6] T. Dhondy, A. Remennikov, M. Neaz Shiekh. (2019). Benefits of using sea sand and seawater in concrete: a comprehensive review. *Australian Journal of Structural Engineering*, 20(4), 280-289.https://doi.org/10.1080/13287982.2019.1659213

[7] J. Xiao, C. Qiang, A. Nanni, K. Zhang. (2017). Use of sea-sand and seawater in concrete construction: Current status and future opportunities. *Construction and Building Materials*, 155, 1101-1111. https://doi.org/10.1016/j.conbuildmat.2017.08.130

[8] P. Hawkins, P. Tennis, R. Detwiler. (2005). The Use of Limestone in Portland Cement, A State-of-the-Art Review. PCA Engineering Bulletin, 227.

[9] D. Zhang, J. Jiang, Z. Zhang, L. Fang, Y. Weng, L. Chen, D. Wang. (2024). Comparative analysis of sulfate resistance between seawater sea sand concrete and freshwater desalted sea sand concrete under different exposure environments. *Construction and Building Materials*, 416, 135146. https://doi.org/10.1016/j.conbuildmat.2024.135146

[10] S. Rathnarajan, P. Sikora. (2023). Seawater-mixed concretes containing natural and sea sand aggregates – A review. *Results in Engineering*, 20, 101457. https://doi.org/10.1016/j.rineng.2023.101457

[11] J. Sobhani, F. Jafarpour, F. Firozyar, A.R. Pourkhorshidi. (2022). Simulated C3A Effects on the Chloride Binding in Portland Cement with NaCl and CaCl2 Cations. *Journal of Civil Engineering and Materials Application*, 6(1), 41-54. https://doi.org/10.22034/jcema.2022.328603.1080

[12] Y. Cheng, Z. Li, X. Huang, X. Bai. (2017). Effect of Friedel's salt on strength enhancement of stabilized chloride saline soil. *Journal of Central South University*, 24, 937-946. https://doi.org/10.1007/s11771-017-3496-7

[13] K.T. Nguyen, T.A. Le, K. Lee. (2018). Evaluation of the mechanical properties of sea sand-based geopolymer concrete and the corrosion of embedded steel bar. *Construction and Building Materials*, 169, 462-472. https://doi.org/10.1016/j.conbuildmat.2018.02.169

[14] B. Nematollahi, K. Ichimiya, M. Kunieda. (2023). Recent advances in high-performance fiber-reinforced geopolymer composites for resilient and sustainable construction. *Journal of Advanced Concrete Technology*, 21, 1129-1146. https://doi.org/10.3151/jact.21.S1

[15] J. Davidovits. (1993). Geopolymer cement to minimize carbon-dioxide greenhouse-warming. *Ceramic Transactions*, 37(1), 165-182.

[16] R.M. Andrew. (2019). Global CO2 emissions from cement production, 1928–2018. *Earth System Science Data*, 11(4), 1675-1710. https://doi.org/10.5194/essd-11-1675-2019

[17] H.U. Ahmed et al. (2022). Geopolymer concrete as a cleaner construction material: An overview on materials and structural performances. *Cleaner Materials*, 5, 100111. https://doi.org/10.1016/j.clema.2022.100111

[18] M.I.A. Aleem, P.D. Arumairaj. (2012). Geopolymer concrete - A review. *International Journal of Engineering Sciences & Emerging*

Technologies, 1(2), 118-122. doi: 10.7323/ijeset/v1_i2_14

[19] M.T. Ghafoor, C. Fujiyama, K. Maekawa. (2021). Mix design processing for self-compacting geopolymer mortar. *Journal of Advanced Concrete Technology*, 19(11), 1133-1147. https://doi.org/10.3151/jact.19.1133

[20] S. Sbahieh, G. McKay, S.G. Al-Ghamdi. (2023). Comprehensive Analysis of Geopolymer Materials: Properties, Environmental Impacts, and Applications. *Materials*, 16(23), 7363. https://doi.org/10.3390/ma16237363

[21] Banoth Gopalakrishna, D. Pasla. (2024). Durability Performance of Recycled Aggregate Geopolymer Concrete Incorporating Fly Ash and Ground Granulated Blast Furnace Slag. *Journal of Materials in Civil Engineering*, 36(4), 04024037.https://doi.org/10.1061/JMCEE7.MTENG-17067

[22] K. Arbi, M. Nedeljković, Y. Zuo, G. Ye. (2016). A review on the durability of alkali-activated fly ash/slag systems: Advances, issues, and perspectives. *Industrial and Engineering Chemistry Research*, 55(19), 5439-5453. DOI: 10.1021/acs.iecr.6b00559

[23] C. Arenas, Y. Luna-Galiano, C. Leiva, L.F. Vilches, F. Arroyo, R. Villegas, C. Fernández-Pereira. (2017). Development of a fly ash-based geopolymeric concrete with construction and demolition wastes as aggregates in acoustic barriers. *Construction and Building Materials*, 134, 433-442. https://doi.org/10.1016/j.conbuildmat.2016.12.119

[24] I. Garcia-Lodeiro, A. Palomo, A. Fernández-Jiménez, D.E. Macphee. (2011). Compatibility studies between N-A-S-H and C-A-S-H gels. Study in the ternary diagram Na2O-CaO-Al2O3-SiO2-H2O. *Cement and Concrete Research*, 41(9), 923-931. https://doi.org/10.1016/j.cemconres.2011.05.006

[25] B. Gopalakrishna, P. Dinakar. (2023). Mix design development of fly ash-GGBS based recycled aggregate geopolymer concrete. *Journal of Building Engineering*, 63, 105551. https://doi.org/10.1016/j.jobe.2022.105551

[26] A.İ. Uğurlu, M.B. Karakoç, A. Özcan. (2021). Effect of binder content and recycled concrete aggregate on freeze-thaw and sulfate resistance of GGBFS based geopolymer concretes. *Construction and Building Materials*, 301, 124246. https://doi.org/10.1016/j.conbuildmat.2021.124246

[27] J. Zhao, Z. Jiang, Z. Lu, Y. Tan, S. Li, B. Zhang, J. Xie. (2024). Coupling Effects of Seawater Immersion and Prestressing on the Durability of BFRP Bars Embedded in Seawater–Sea Sand Geopolymer Mortars. *Journal of Materials in Civil Engineering*, 36(4), 04024049. https://doi.org/10.1061/JMCEE7.MTENG-17106

[28] X. Lyu, N. Robinson, M. Elchalakani, M.L. Johns, M. Dong, S. Nie. (2022). Sea sand seawater geopolymer concrete. *Journal of Building Engineering*, 50, 104141. https://doi.org/10.1016/j.jobe.2022.104141

[29] S. He, C. Jiao, Y. Niu, S. Li. (2022). Utilizing of coral/sea sand as aggregates in environment-friendly marine mortar: Physical properties, carbonation resistance and microstructure. *Case Studies in Construction Materials*, 16, e00981.https://doi.org/10.1016/j.cscm.2022.e00981

[30] J. Yang, D. Xu, J. Shen, H. Wei, R. Wang, X. Xiao. (2022). Effect of coral sand powders and seawater salinity on the impact mechanical properties of cemented coral sand. *Soils and Foundations*, 62(5), 101206. https://doi.org/10.1016/j.sandf.2022.101206

[31] W. Kunther, B. Lothenbach, J. Skibsted. (2015). Influence of the Ca/Si ratio of the C–S–H phase on the interaction with sulfate ions and its impact on the ettringite crystallization pressure. *Cement and Concrete Research*, 69, 37-49.

https://doi.org/10.1016/j.cemconres.2014.12.002

[32] J. Wang, P.A.M. Basheer, S.V. Nanukuttan, A.E. Long, Y. Bai. (2016). Influence of service loading and the resulting micro-cracks on chloride resistance of concrete. *Construction and Building Materials*, 108, 56-66. https://doi.org/10.1016/j.conbuildmat.2016.01.005

[33] B. Da, H. Yu, H. Ma, Y. Tan, R. Mi, X. Dou. (2016). Chloride diffusion study of coral concrete in a marine environment. *Construction and Building Materials*, 123, 47-58. https://doi.org/10.1016/j.conbuildmat.2016.06.135

[34] Nordtest. (1989). Concrete, repairing materials and protective coating: Embedded steel method, chloride permeability (NT BUILD 356).

[35] J. Temuujin, A. Minjigmaa, M. Lee, N. Chen-Tan, A. Riessen. (2011). Characterization of class F fly ash geopolymer pastes immersed in acid and alkaline solutions. *Cement and Concrete Composites*, 33(10), 1086-1091. https://doi.org/10.1016/j.cemconcomp.2011.08.008

[36] A. Rafeet, R. Vinai, M. Soutsos, W. Sha. (2019). Effects of slag substitution on physical and mechanical properties of fly ash-based alkali activated binders (AABs). *Cement and Concrete Research*, 122, 118-135. https://doi.org/10.1016/j.cemconres.2019.05.003

[37] A. Noushini, A. Castel, J. Aldred, A. Rawal. (2020). Chloride diffusion resistance and chloride binding capacity of fly ash-based geopolymer concrete. *Cement and Concrete Composites*, 105, 103290. https://doi.org/10.1016/j.cemconcomp.2019.04.006